El Niño/Southern Oscillation during the 4.2 ka event recorded by growth rates of corals from the North South China Sea

Shaohua Dang[1, 2, 3], Kefu Yu[1, 2, 3*], Shichen Tao[4], Tao Han[4], Huiling Zhang[5], Wei Jiang[1, 2, 3]

[1] Guangxi Laboratory on the Study of Coral Reefs in the South China Sea, Guangxi University, Nanning 530004, China

[2] Coral Reef Research Center of China, Guangxi University, Nanning 530004, China

[3] School of Marine Sciences, Guangxi University, Nanning 530004, China

[4] South China Sea Institute of Oceanology, Chinese Academy of Sciences, Guangzhou 510301, China

[5] College of Ocean Engineering, Guangdong Ocean University, Zhanjiang 524088, China

Abstract

The 4.2 ka event that occurred during the period from 4 500–3 900 a BP was characterized by cold and dry climates and resulted in the collapse of civilizations around the world. The cause of this climatic event, however, has been under debate. We collected four corals (*Porites lutea*) from Yongxing Island, Xisha Islands, South China Sea, dated them with the U-series method, and measured the annual coral growth rates using X-ray technology. The dating results showed that the coral growth ages were from 4 500–3 900 a BP, which coincide well with the period of the 4.2 ka event. We then reconstructed annual sea surface temperature anomaly (SSTA) variations based on the coral growth rates. The growth rate-based SSTA results showed that the interdecadal SSTA from 4 500–3 900 a BP was lower than that during modern times (1961–2008 AD). A spectral analysis showed that the SSTA variations from 4 500–3 900 a BP were under the influence of El Niño-Southern Oscillation (ENSO) activities. From 4 500–4 100 a BP, the climate exhibited La Niña-like conditions with weak ENSO intensity and relatively stable and lower SSTA amplitudes. From 4 100–3 900 a BP, the climate underwent a complicated period of ENSO variability and showed alternating El Niño- or La Niña-like conditions at interdecadal time scales and large SSTA amplitudes. We speculate that during the early and middle stages of the 4.2 ka event, the cold climate caused by weak ENSO activities largely weakened social productivity. Then, during the end stages of the 4.2 ka event, the repeated fluctuations in the ENSO intensity caused frequent extreme weather events, resulting in the collapse of civilizations worldwide. Thus, the new evidence obtained from our coral records suggests that the 4.2 ka event as well as the related collapse of civilizations were very likely driven by ENSO variability.

Key words: 4.2 ka event, ENSO variability, SSTA, coral growth rate, Xisha Islands

---

1 Introduction

The occurrence of the widespread 4.2 ka climactic event was characterized by intense cooling and aridity across the mid-low latitudes in the Northern Hemisphere (Walker et al., 2012; Weiss et al., 1993; Wanner et al., 2008, 2011, 2015), including rapid cooling in Europe (Mackay et al., 2003), centennial to decadal megadroughts in North America (Booth et al., 2005), rapid cooling in the western Pacific and typical climate transformations with cooling and drying across the Mediterranean region to the Indian Peninsula (Kathayat et al., 2017; Nakamura et al., 2016; Staubwasser et al., 2003; Walker et al., 2012; Weiss, 2016; Wang et al., 1996). These climate anomalies are considered to be associated with the collapse of human civilizations during that period (Weiss, 2016). Due to its widespread influences, the 4.2 ka event is defined as the boundary between the top Holocene and the late Holocene (Gibbard, 2018; Walker et al., 2012). However, the driving mechanisms of this event are still under debate. Some studies have suggested that conditions in the North Atlantic climate generated this break (Deininger et al., 2017; Olsen et al., 2012; Ramos-Román et al., 2018; Yan and Liu, 2019; Zhang et al., 2018); other studies have suggested that the spatial patterns of the Intertropical Convergence Zone (ITCZ), namely, a north-south meridional shift and contraction of the ITCZ, resulted in this event (Griffiths et al., 2010; Li et al., 2018; Tan, 2018a); while a third group of studies have suggested that an unusual El Niño-Southern Oscillation (ENSO) mode triggered this climatic variation (Booth et al., 2005; Toth et al., 2012, 2015). Additionally, clear cooling and drought signals are not observed in some records of the 4.2 ka event, although high-moisture features during this event have been demonstrated (Kathayat et al., 2017; Li et al., 2018; Roland et al., 2014; Tan et al., 2018 a,b; Wu et al., 2012; Xu et al., 2015).

Regarding the climate conditions in the East Asian continent during the 4.2 ka event, most studies have focused on the hydro-

---

logical changes associated with the Asian monsoon system. In existing paleo-hydrology reconstructions (Chen et al., 2015; Liu et al., 2015, 2017; Rao et al., 2016; Zhao et al., 2010), a clear discrepancy occurs between northern and southern China. Although most of northern China experienced drought conditions (Chen et al., 2015; Zhao et al., 2010), great flood events might have occurred ca. 4 000 a BP in the Huanghe (Yellow) River basin (Tan et al., 2018 b; Wu et al., 2016). Meanwhile, abnormally moist climatic features occurred in the Changjiang (Yangtze) River basin and southern China at centennial timescales (Tan et al., 2018 a ; Wu et al., 2012; Xu et al., 2015). Most of these terrestrial high-resolution paleo-climate records are based on the oxygen isotopes of stalagmites, although their climate implications in southern China are still elusive (Liu et al., 2015, 2017; Rao et al., 2016). In comparison, direct high-resolution paleo-temperature records of the 4.2 ka event are sparse. Hence, a comprehensive understanding of paleo-temperature records for the 4.2 ka event in East Asia is still needed and may be more persuasive than hydrological reconstructions.

As one of the major water vapor sources for rainfall in the East Asian continent, the South China Sea has a profound impact on East Asian climate conditions (Wang et al., 2009; Zhou and Chan, 2007). Corals are widely distributed in the South China Sea and can provide insights into the Holocene climate changes in the surrounding region (Yu, 2012). The aragonitic skeletons of corals are suitable for high-precision uranium dating, and their clear annual layers can indicate annually resolved climate information. Specifically, the annual growth rates of coral can represent the sea surface temperature (SST) under certain circumstances (Lough and Cooper, 2011; Saenger et al., 2009; Vásquez-Bedoya et al., 2012). A number of studies have indicated a positive linear relationship between the SST in the habitat of corals (*Porites lutea*) in the South China Sea and their annual growth rates (Huang et al., 2013; Lin et al., 2018; Nie et al., 1997, 1999; Zhang, 2013; Zhang et al., 2014, 2017). Accordingly, we reconstructed annually resolved SST variations based on the growth rates of five fossil corals (*Porites lutea*) for the period 4 500–3 900 a BP. In most cases, the coral samples during the 4.2 ka period are almost entirely covered by later-formed coral reefs, which will grow over previously formed corals during their development. Consequently, samples that cover the whole period of the 4.2 ka event are difficult to obtain in the field, which is an important reason for the lack of authoritative reports on the whole 4.2 ka event recorded in corals.

2 Research area and sample details

Yongxing Island is located in the eastern part of the Xisha Islands in the northern part of the South China Sea (SCS) (Fig. 1). This area is dominated by the tropical monsoon climate regime. According to data from the ocean observatory on Yongxing Island for 1961–2008 AD, the annual average SST was 27.4°C. In the most recent annual cycle, the highest SST was 29.8°C, which occurred from May to September, and the lowest SST was 24.7°C, which occurred from December to February the next year. In this sea area, mainly southwest winds prevail in summer and autumn because of the Asian summer monsoon system and mainly northeast winds prevail in winter and early spring because of the East Asian winter monsoon (Wang et al., 2009).

The coral (*Porites lutea*) samples of our research, including YX10-60-2, YX10-38 and YX10-12 were collected in the southeast part of Yongxing Island in 2008 AD. The coral cores were cut into 8 mm thick slabs along the main growth axis and washed with fresh water. To acquire clear annual band graphs, we produced X-radiographs of these slabs. As shown in Fig. 2, these corals show clear annual bands with high and low densities similar to tree ring bands. A successive high and low density band was considered to represent the growth distance of one year. After these physical steps, we selected 0.05–0.1 g fragments at the top/bottom of the samples along the major growth axis and sent the fragments to the Radiogenic Isotope Facility, School of Earth and Environmental Sciences, University of Queensland to obtain chronological data via a U-series analysis using a Thermal Ionization Mass Spectrometer (TIMS). The details of this method were reported by Yu (Yu et al., 2006). The dating results of the samples are listed in Table 1. Subsequently, the chronological ages of these samples was obtained via counting the annual layers along the growth orientation. The detailed ages are marked on left sides of the X-radiographs (Fig. 2).

3 Construction and demonstration of a coral growth rate thermometer

3.1 *Measurement of coral growth rates*

Measurements of coral growth rate data can be obtained by analysing X-radiographs. In X-radiographs, the annual linear extension is the distance between successive high and low-density peaks on the major growth axis. "Sante DICOM Viewer Free" software was used to analyse these X-radiographs because this software was associated with the X-ray machine. In each sample, three main growth axes or more were measured and the meas-
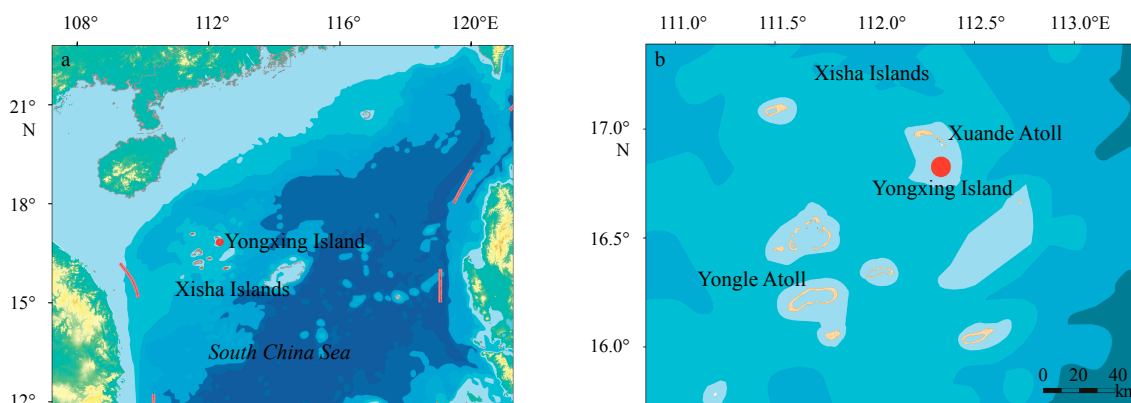

Fig. 1. Research area and sample site. a. Geographical map of the northern part of the SCS, with the red dot indicating the location of Yongxing Island; and b. map of the Xisha Islands, with the red dot indicating the location of the sample site on the Yongxing Island.
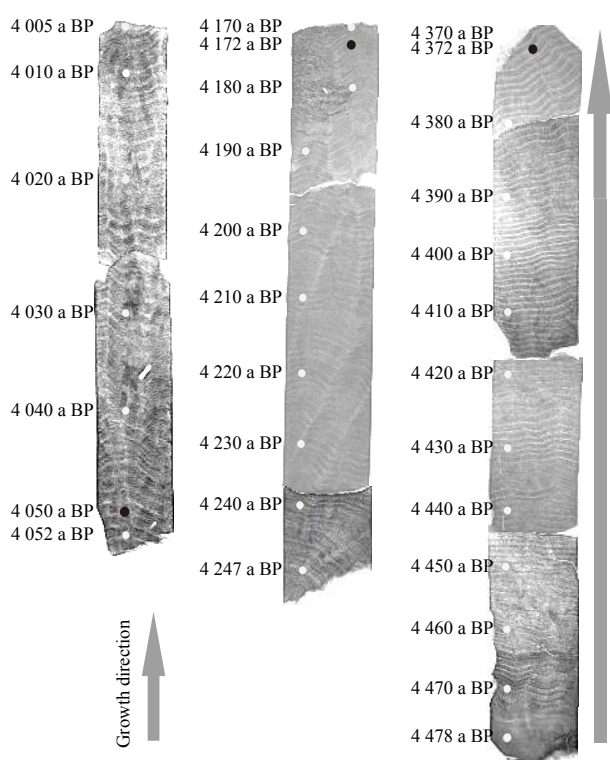
Fig. 2. X-radiography with dating points. The black dots represent the dating layer, and the grey dots represent the speculated chronological ages based on dating points.

ured results were then averaged. All the measurement results were accurate to two decimal places.

The X-radiograph analysis revealed 108 annual bands ranging from 4 478–4 370 a BP in YX10-60-2, 78 annual bands ranging from 4 247–4 170 a BP in YX10-38, and 109 annual bands ranging from 4 052–4 005 a BP in YX10-12. We also spliced our samples with the samples from Zhang (2013) and Zhang et al. (2014), which ranged from 4 004–3 960 a BP and 3 950–3 909 a BP. Our research period spanned 4 478–3 909 a BP. The individual annual growth rate results, which had a mean value of 8.11 mm/a, are shown in Fig. 3a. The annual growth rates of the individual colonies spanned from 4.82 to 9.67 mm/a, 3.66 to 7.53 mm/a, 3.97 to 14.41 mm/a, 6.61 to 13.83 mm/a and 8.52 to 13.11 mm/a over this time period. We then analysed the relationship between modern coral growth rates (1961–2008 AD) (Zhang et al., 2014) and the physical environment. Over the past century or more, the coral growth rates ranged from 7 to 15 mm/a, with a mean value of 11 mm/a; and from 1961–2008 AD, the rates ranged from 11.81 to 17.58 mm/a, with a mean value of 11.85 mm/a (Zhang et al., 2014).

3.2 *Relationship between coral growth rate and SST*

Changes in the coral physical environment, including changes in the sea surface salinity (SSS), solar radiation, nutri-

ents from upwelling or terrestrial runoff and SST, are known to drive variability in coral annual growth rates, with SST accounting for the primary changes in coral growth rates under most conditions (Lough and Barnes, 1997, 2000; Lough and Cooper, 2011). The past 220 a of SST variations have been successfully reconstructed based on the linear relationship between the instrumental SST and modern coral growth rates of the Xisha Islands (Nie et al., 1997, 1999). In addition, the SST variations from the top to late Holocene in the Xisha Islands have been established according to the linear relationship between instrumental SST and modern coral growth rates (Zhang et al., 2014). However, the reliability of these two linear relationships must be confirmed because the contributions of other physical environmental elements to coral annual linear extensions are less well known. Due to the location of the Xisha Islands, the influence of nutrients and pollutants input from terrestrial runoff and upwelling can be neglected. Therefore, we analysed the linear correlation between the modern coral growth rate and the SSS data, SST data and solar radiation. The SSS and SST data were obtained from ocean observations of Yongxing Island, and the solar radiation data were derived from the website https://www.esrl.noaa.gov/psd/data/gridded. As shown in Fig. 4a, the SST series present a significant correlation (R^2=0.61, P<0.01) with the coral growth rates from 1961–2008 AD at an annual time scale (Zhang et al., 2014). The correlation results between the annual coral growth rates and SSS (R^2=0.01, P<0.01) and solar radiation (R^2=0.07, P<0.01) are generally lower than those between the annual coral growth rates and SST. Therefore, SSS and solar irradiance account for a considerably lower contribution to coral growth rates than SST in the Xisha Islands. Practically, this coral growth rate thermometer, i.e., SST=0.2×L+24.91, is similar to Nie's coral growth rate thermometer, SST=0.225×L+24.772. Only a small error of approximately 0.16°C is observed between these thermometers in the annually resolved SST over the most recent century (Nie et al., 1997, 1999; Zhang et al., 2014). Considering these facts, we used the linear correlation results for coral growth rates from Zhang's research (Zhang et al., 2014) to reconstruct the SST variations and then analysed the SST anomalies of each sample during the period of the 4.2 ka event.

4 Results and discussion

4.1 *Characteristics of reconstructed SST variations (4 478–3 909 a BP)*

Based on these four spliced periods as a whole (Fig. 3b), the amplitudes of the reconstructed SST anomalies have undergone complicated variations. The fluctuation range was small and stable at an annual scale and presented values of 1.1°C and 0.75°C from 4 478–4 370 a BP ("early stage of the 4.2 ka event" herein) and 4 247–4 170 a BP ("top stage of the 4.2 ka event" herein), respectively. However, sharp fluctuations from 2.2°C to 0.9°C were observed from 4 052–3 909 a BP ("end stage of the 4.2 ka event" herein). These findings are well correlated with the contemporary maximum temperature amplitude (~2°C) of the Chinese mainland (Fang and Hou, 2011). Additionally, the interdecadal variations processed by a moving average of SST anom-

Table 1. U-Th series ages of coral samples from the Yongxing Island

| Sample name	U/10^{-6}	$^{232}Th/10^{-9}$	$^{230}Th/^{232}Th$	$^{230}Th/^{238}U$	$^{234}U/^{238}U$	Uncorrected age/ka BP	Corrected age/ka BP	Initial ratios /$^{234}U/^{238}U$
YX10-12	2.662 7±0.001 4	1.43±0.002	233.22±0.9	0.041 9±0.000 2	1.147 3±0.001 0	4.064±0.016	4.05±0.017	1.149±0.001
YX10-38	2.518 1±0.002 1	0.24±0.001	1372.48±7.06	0.043 0±0.000 2	1.145 7±0.000 8	4.174±0.018	4.172±0.018	1.147 4±0.000 8
YX10-60-2	2.436 9±0.001 3	0.36±0.001	937.56±3.72	0.045 0±0.000 2	1.145 9±0.001 1	4.376±0.017	4.372±0.017	1.147 7±0.001 2
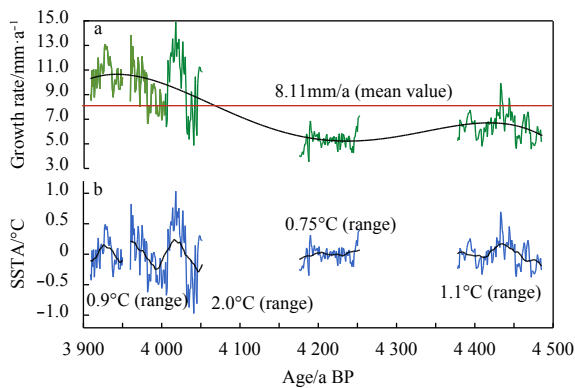
Fig. 3. Coral growth rate (a) and reconstructed SSTA (b) results. The light green lines were cited from Zhang's research (Zhang et al., 2014). The black splines in Figs 3a and b represent the variation tendency of the growth rates and 31 a moving average of the reconstructed SSTA, respectively.

alies over 31 a displayed a similar tendency, with stable SSTA during the initial and top phases and unstable SSTAs during the
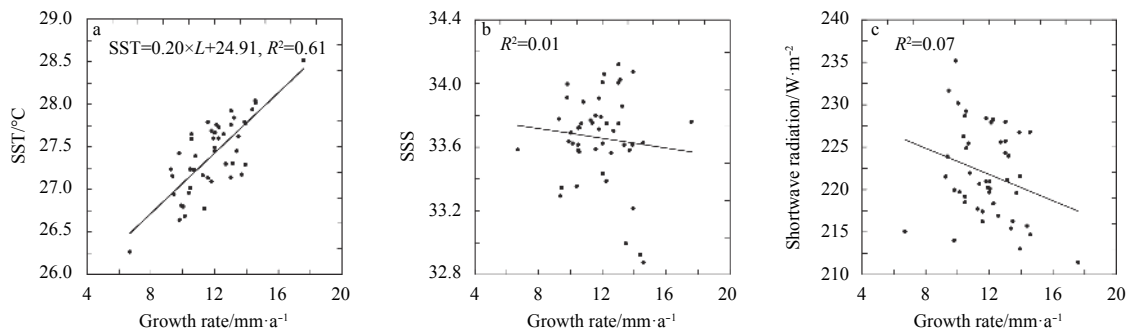
end phase. We calculated the amplitudes of the SST anomalies in a sliding 31 a window with 1 a steps to precisely determine their interdecadal changes (Fig. 7c). The results indicated that the range of SSTA amplitudes during the end stage was larger than that of the other stages except for the modern period (1961–2008 AD). These four coral-based SST series were then analysed using a power spectral analysis to deeply investigate the SST variations. As shown in Fig. 5, at interannual timescales, 3–7 a periods of variation were observed, and they were supported by a high confidence level of 90% or more.

4.2 *Impact of the El Niño and Southern Oscillation (ENSO) variability*

Global interannual climate change is dominated by ENSO variability (Trenberth and Caron, 2000). The pronounced interannual period of SST variations ranging from 2–8 a is the result of typical ENSO modes (Ropelewski and Halpert, 1987); hence, we assumed that periods of 3–7 a in the spectral analysis may indicate the ENSO signals at that time (Wang et al., 2017). Consequently, the responses to ENSO variability in our annually resolved SST data during the 4.2 ka event must be investigated.

Fig. 4. Relationship between the coral growth rate and the SST (a), SSS (b) and shortwave radiation (c) on the Yongxing Island, respectively. The coral growth rate data are from Zhang's research (Zhang et al., 2014).

4.2.1 *Observed SST response to ENSO variability*

The spectral analysis demonstrated principle spectral peaks related to modern monthly SST variations in the Xisha Islands between 3 and 7 a (Yan et al., 2017). A high correlation (0.55, *P*<0.01) between the SCS SST anomalies and the ENSO index was observed when the SCS SST anomalies were lagged by approximately 5 months because of the influence of tropical atmospheric bridges (Klein et al., 1999). At interannual timescales, when the Xisha Islands SST anomalies were lagged by approximately 1 a, a significant correlation (*R*=0.54, *P*<0.01) between the Xisha Islands) SST anomalies and the Niño3 SST anomalies occurred from 1961–2008 AD (Fig. 6a). To quantify the responses of Yongxing Island's SST excursions relative to ENSO activity, we performed 3–7 a bandpass filtering on the annual SST anomaly variations from 1961–2008 AD to remove the noise signal. After filtering, we selected the peak values to construct the responses to ENSO events (Fig. 6). We defined positive or negative excursions as responses to El Niño events or La Niña events, and these excursions reflected 13 El Niño events and 11 La Niña events, respectively. According to the Meteorological Industry Standard for the "Identification method for El Niño/La Niña events", published by the China Meteorological Administration (CMA, 2017), more than 15 El Niño events and 10 La Niña events occurred from 1961–2007 AD. The precision rate reached 85% because two false

negative peaks were identified in 2 El Niño events and a false positive peak was identified in 1 La Niña event. Specifically, the Xisha Islands experienced high temperatures when El Niño events occurred and low temperatures when La Niña events occurred (Yan et al., 2010; Liu et al., 2013). Otherwise, in the last millennium, climate variations in the Xisha Islands also corresponded to ENSO variability to a large extent (Yan et al., 2011a, b). Therefore, SST variations in the Xisha Islands could capture most ENSO events.

4.2.2 *Pattern of 4.2 ka ENSO variability evolution*

To evaluate the responses to ENSO variability during the 4.2 ka event, we extracted the series for ENSO variations (Fig. 7a) from the reconstructed SST anomalies and instrumental SST anomalies using a 3–7 a bandpass filter. We then calculated the number of ENSO events, which were classified by the positive or negative peaks, in a sliding window of 31 a. Subsequently, sliding this time window per 1 a enabled us to acquire interdecadal variations for ENSO activities (Fig. 7d). Additionally, similar to Cobb's research (Cobb et al., 2013), we calculated the relative ENSO variance in a sliding 31 a window with 1 a steps to assess the interdecadal strength of ENSO variability (Fig. 7b) relative to the period from 1968–1998 AD ('modern stage' herein) because of its highest level of ENSO variance (29%). In the modern stage, a high
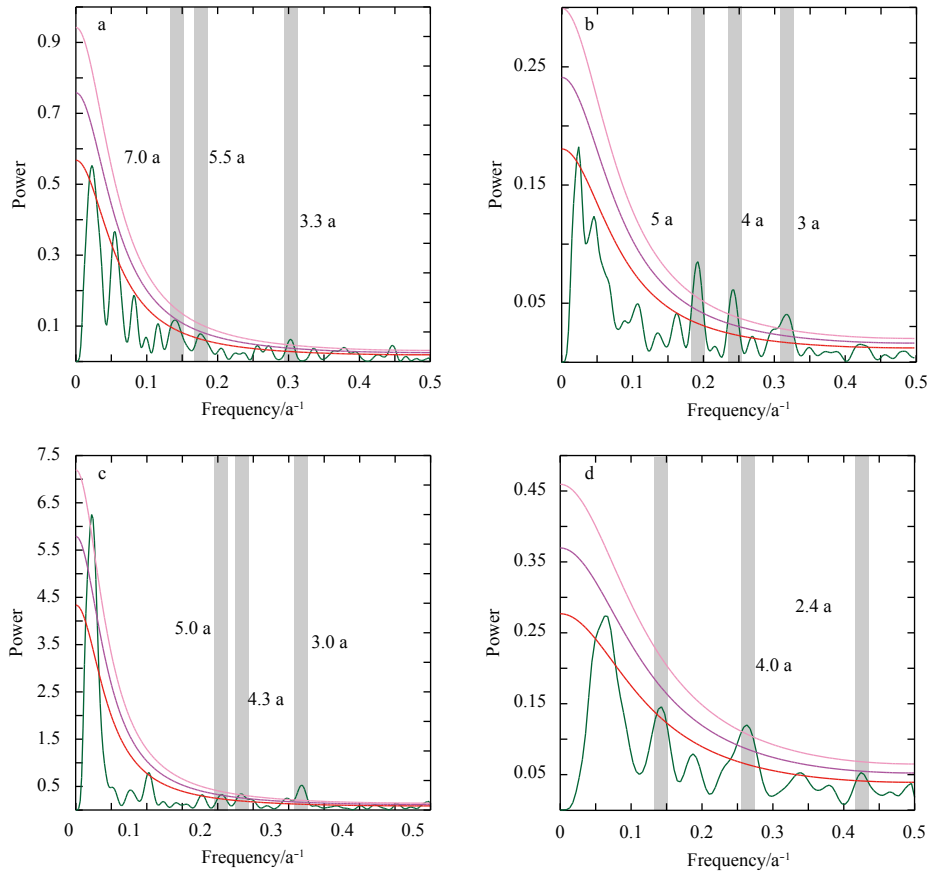
Fig. 5. Results of the power spectral analysis. The chronology messages of Figs 5a, b, c and 5d are 4 478–4 370 a BP, 4 247–4 170 a BP, 4 052–3 960 a BP and 3 950–3 910 a BP, respectively. The light pink, dark pink, and red lines represent confidence levels of 80%, 90% and 95%, respectively.
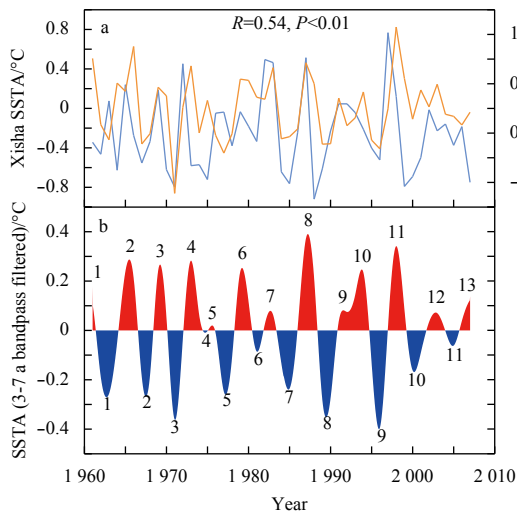

Fig. 6. Observed SST response to ENSO variability. a. Comparison between the instrumental SST records (yellow) of the Xisha Islands and Niño 3 SST records (blue) from 1961–2008 AD; and b. responses to ENSO events for instrumental SST (3–7 a bandpass filtered). The red peaks represent El Niño events, and the blue peaks represent La Niña events.

level of interdecadal SSTA amplitudes corresponded to a greater occurrence of El Niño events than La Niña events.
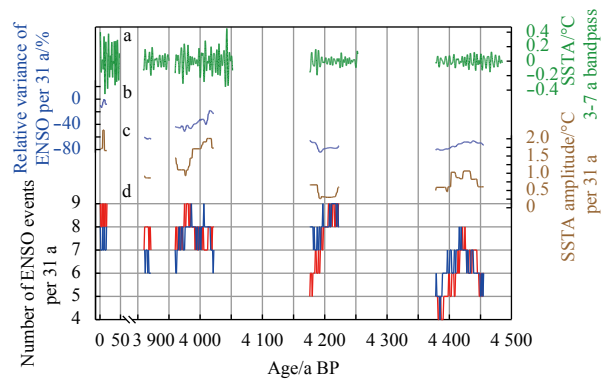

Fig. 7. Green curve shows the variation of the 3–7 a bandpass filtering results (a). Light blue curve shows the strength of the ENSO activities (b). Brown curve shows the reconstructed SST anomaly (c). Red and blue curves show the interdecadal changes in warm and cold ENSO events (d).

Relative to the modern stage, the medial relative ENSO variance was reduced by 73% during the early stage. This decreasing trend was mainly manifested by decreased numbers of ENSO events in the sliding 31 a window, which also varied synchronously with the SSTA amplitudes in the 31 a sliding window. During the modern stage, 8–9 El Niño events and 7–8 La Niña events were captured in the Xisha Islands SST excursions. However, 5–6 ENSO events were captured in the sliding windows during the

early stage of the 4.2 ka event, including a transition from El Niño-like conditions to La Niña-like conditions. In addition, we found that a 175 a coral-based ENSO record was consistent with our records because its ENSO variance declined by 79% (McGregor et al., 2013). This weak ENSO record also indicated an increasing east-west gradient of SST in the zonal Pacific because of external forcing (Koutavas and Joanides, 2012; McGregor et al., 2013). Therefore, the decreasing SSTA amplitudes in the Xisha Islands were associated with weak ENSO variability during the early stage of the 4.2 ka event.

The medial ENSO intensity dropped to the lowest level from 4 247–4 170 a BP as the relative ENSO variance decreased by 76% compared with the modern stage. In addition, more numerous cold ENSO events occurred in the top stage than the early stage of the 4.2 ka event. In the 31 a sliding window, the number of La Niña events varied from 7 to 9 while the number of El Niño events decreased from 9 to 5 during this stage. Therefore, La Niña-like conditions can be verified in the top stage of the 4.2 ka event because the number of La Niña events was higher than the number of El Niño events. Furthermore, the number of La Niña events in this stage was higher than that of the modern stage. Simultaneously, the interdecadal SSTA amplitudes were at the lowest level compared with the other stages, which correlated well with the relative ENSO variance.

During the end stage of the 4.2 ka event, the ENSO intensity surpassed that of the previous stages. Compared with the modern stage, the medial relative ENSO variance decreased by 37%. The strongest level occurred at ca. 4 000 a BP because the reduction in the relative ENSO variance was only 18%. These findings were assumed by the increasing occurrence of warm or cold ENSO events, which increased from 6 to 9 events per 31 a. An intricate ENSO variation mode revealed by the alternating manipulation modes of the El Niño-like condition and the La Niña-like condition at interdecadal timescale covered the majority of the end stage, and the El Niño-like condition was prevalent at the end part. Therefore, the large fluctuations in SSTA at interdecadal time scales during this stage were generated by repeated fluctuations in ENSO intensity and the transition from La Niña-like conditions to El Niño-like conditions.

4.2.3 *ENSO-related extreme weather events and civilization collapse*

Because El Niño (La Niña) events correspond to positive (negative) SST excursions in the Xisha Islands (Yan et al., 2010), we inferred that the global cooling during the 4.2 ka event was largely attributable to La Niña-like conditions. With the prevalence of La Niña-like conditions, the ability of humans to tolerate the environment may have declined because the anthropic crop yield likely decreased under the cooling and drought conditions at that time (4 500–4 100 a BP). After these two stages, extreme weather events were enhanced likely due to the combination of the relatively strong ENSO variance and the transitions from La Niña-like conditions to El Niño-like conditions. Extreme weather events and the associated natural hazards generated by the strong ENSO variability have caused great harm to human development in the last few decades. For instance, a super El Niño incident in 1982 severely reduced crop yields because of the associated drought conditions (Iizumi et al., 2014). A strong El Niño event in 1998 led to synchronous flood disasters across mainland China (Huang et al., 2000). A notable snowstorm in southern China in 2007 and 2008 was also considered to be related to the La Niña incident in that year (Wang et al., 2008). Thus, even in modern times, humans have insufficient resilience under such

dramatic climate changes; moreover, the resilience of humans who lived in the early days of the civilization was much lower than that of modern humans.

Several archaeological reconstructions have indicated that numerous civilization collapses occurred because of the extreme climate conditions in the 4.2 ka event. In southern China, the collapse of the Liangzhu culture was attributed to the frequent flood and drought disasters at that time (Shi et al., 2008). In northern China, the enhanced climatic pattern of northern droughts and southern floods prompted a decline in civilizations during the 4.2 ka event (Wu and Liu, 2004; Wu et al., 2016), whereas the probability of flooding in northern China was higher than that in southern China ca. 4 000 a BP (Tan et al., 2018 b; Cui and Zhou, 2003). Compared with the ordinary climatic patterns of northern droughts and southern floods or southern floods and northern droughts in China (Ding et al., 2008), the results of these archaeological records from China indicated that the climatic pattern during the 4.2 ka event, especially at its end stage, was likely influenced by strong ENSO variability. These synchronous extreme weather events and natural disasters across northern to southern China may confirm the effects of ENSO variability on the East Asian climate during the 4.2 ka event. These extreme weather events may have ultimately contributed to the rise and collapse of civilizations.

5 Conclusions

In this study, we first reconstructed the annually resolved SSTA variations in the Xisha Islands based on coral (*Porites lutea*) growth rates during the 4.2 ka event. We then extracted the ENSO signal in the coral growth rate record and discussed the ENSO variability at interdecadal time scales. The three main findings were as follows.

(1) The reconstruction of SSTA based on coral growth rates showed that the interdecadal amplitudes of SSTA were smaller than that during modern times over the majority of the 4.2 ka event. A stable mode represented by a small amplitude range was captured from 4 500–4 100 a BP, and an unstable mode represented by a large amplitude range was captured from 4 100–3 900 a BP.

(2) The SST variations in the Xisha Islands mainly indicate ENSO variability during the 4.2 ka event. The stable and lower SSTA amplitudes were mainly controlled by weak ENSO activities and La Niña-like conditions during the early and top stages of the 4.2 ka event, whereas the unstable and higher SSTA amplitudes were due to relatively strong ENSO activities and a transition from La Niña-like conditions to El Niño-like conditions during the end stage of the 4.2 ka event. Furthermore, this transition phase was the main cause of the alternating El Niño- or La Niña-like conditions at the interdecadal timescale and the largest SSTA amplitude at that time.

(3) The impact of the 4.2 ka event on the collapse of civilizations was likely due to ENSO variability. During the early and top stages of the 4.2 ka event, the cold climate caused by weak ENSO activities largely weakened social productivity. During the end stage of the 4.2 ka event, increasingly extreme weather events caused by repeated fluctuations in the ENSO intensity further weakened the tolerance of humans to their living environments, which may have led to the collapse of civilizations worldwide.

References

Booth R K, Jackson S T, Forman S L, et al. 2005. A severe centennial-scale drought in midcontinental North America 4200 years ago and apparent global linkages. The Holocene, 15(3): 321–328, doi: 10.1191/0959683605hl825ft

Chen Fahu, Xu Qinghai, Chen Jianhui, et al. 2015. East Asian summer monsoon precipitation variability since the last deglaciation. Scientific Report, 5: 11186, doi: 10.1038/srep11186

China Meteorological Administration (CMA). 2017. QX/T 370-2017 Identification Method for El Niño/La Niña Events (in Chinese). Beijing: China Meteorological Press, 1–4

Cobb K M, Westphal N, Sayani H R, et al. 2013. Highly variable El Niño-Southern Oscillation throughout the Holocene. Science, 339(6115): 67–70, doi: 10.1126/science.1228246

Cui Jianxin, Zhou Shangzhe. 2003. A study on the floods and the cultures of 4000 years ago. Journal of Lanzhou University (Natural Sciences), 39(3): 94–97

Deininger M, McDermott F, Mudelsee M, et al. 2017. Coherency of late Holocene European speleothem δ¹⁸O records linked to North Atlantic Ocean circulation. Climate Dynamics, 49(1–2): 595–618, doi: 10.1007/s00382-016-3360-8

Ding Yihui, Wang Zunya, Sun Ying. 2008. Inter-decadal variation of the summer precipitation in East China and its association with decreasing Asian summer monsoon. Part I: observed evidences. International Journal of Climatology, 28(9): 1139–1161, doi: 10.1002/joc.1615

Fang Xiuqi, Hou Guangliang. 2011. Synthetically reconstructed Holocene temperature change in China. Scientia Geographica Sinica, 31(4): 385–393

Gibbard P. 2018. Formal subdivision of the Holocene Series/Epoch. http://www.stratigraphy.org/index.php/ics-news-and-meetings/125-formal-subdivision-of-the-Holocene-series-epoch.html (2018-09-24)

Griffiths M L, Drysdale R N, Gagan M K, et al. 2010. Evidence for Holocene changes in Australian-Indonesian monsoon rainfall from stalagmite trace element and stable isotope ratios. Earth and Planetary Science Letters, 292(1–2): 27–38, doi: 10.1016/j.epsl.2010.01.002

Huang Bojin, Yu Kefu, Zhang Huiling, et al. 2013. Sea surface temperature variations during the Middle Rome Warm Period as reconstructed by Poritescoralgrowth rates in the Xisha Islands. Tropical Geography, 33(3): 237–241

Huang Ronghui, Zhang Renhe, Zhang Qingyun. 2000. The 1997/98 ENSO cycle and its impact on summer climate anomalies in East Asia. Advances in Atmospheric Sciences, 17(3): 348–362, doi: 10.1007/s00376-000-0028-3

Iizumi T, Luo Jingjia, Challinor A J, et al. 2014. Impacts of El Niño Southern Oscillation on the global yields of major crops. Nature Communication, 5(1): 3712, doi: 10.1038/ncomms4712

Kathayat G, Cheng Hai, Sinha A, et al. 2017. The Indian monsoon variability and civilization changes in the Indian subcontinent. Science Advances, 3(12): e1701296, doi: 10.1126/sciadv.1701296

Klein S A, Soden B J, Lau N C. 1999. Remote Sea surface temperature variations during ENSO: evidence for a tropical atmospheric bridge. Journal of Climate, 12(4): 917–932, doi: 10.1175/1520-0442(1999)012<0917:rsstvd>2.0.co;2

Koutavas A, Joanides S. 2012. El Niño-southern oscillation Extrema in the Holocene and last glacial maximum. Paleoceanography, 27(4): PA4208, doi: 10.1029/2012PA002378

Li Hanying, Cheng Hai, Sinha A, et al. 2018. Hydro-climatic variability in the southwestern Indian Ocean between 6000 and 3000 years ago. Climate of the Past, 14(12): 1881–1891, doi: 10.5194/cp-14-1881-2018

Lin Lifang, Yu Kefu, Tao Shichen, et al. 2018. Interdecadal variability of sea surface temperature from 1780 to 2013 Recorded in corals from the Huangyan Island in the South China Sea. Haiyang Xuebao, 40(9): 31–42

Liu Jianbao, Chen Shengqian, Chen Jianhui, et al. 2017. Chinese cave δ18O records do not represent northern East Asian summer monsoon rainfall. Proceedings of the National Academy of Sciences of the United States of America, 114(15): E2987–E2988, doi: 10.1073/pnas.1703471114

Liu Jianbao, Chen Jianhui, Zhang Xiaojian, et al. 2015. Holocene East Asian summer monsoon records in northern China and their inconsistency with Chinese stalagmite δ18O records. Earth-Sci-

ence Reviews, 148: 194–208, doi: 10.1016/j.earscirev.2015.06.004

Liu Na, Wang Hui, Ling Tiejun, et al. 2013. The influence of ENSO on sea surface temperature variations in the China seas. Acta Oceanologica Sinica, 32(9): 21–29, doi: 10.1007/s13131-013-0348-7

Lough J M, Barnes D J. 1997. Several centuries of variation in skeletal extension, density and calcification in massive Porites colonies from the Great Barrier Reef: a proxy for seawater temperature and a background of variability against which to identify unnatural change. Journal of Experimental Marine Biology and Ecology, 211(1): 29–67, doi: 10.1016/S0022-0981(96)02710-4

Lough J M, Barnes D J. 2000. Environmental controls on growth of the massive coral Porites. Journal of Experimental Marine Biology and Ecology, 245(2): 225–243, doi: 10.1016/s0022-0981(99)00168-9

Lough J M, Cooper T F. 2011. New insights from coral growth band studies in an era of rapid environmental change. Earth-Science Reviews, 108(3–4): 170–184, doi: 10.1016/j.earscirev.2011.07.001

Mackay A, Battarbee R, Birks J, et al. 2003. Global Change in the Holocene. London: Arnold London Press, 242–263, doi: 10.1002/jqs.868

McGregor H V, Fischer M J, Gagan M K, et al. 2013. A weak El Niño/Southern Oscillation with delayed seasonal growth around 4, 300 years ago. Nature Geoscience, 6(11): 949–953, doi: 10.1038/NGEO1936

Nakamura A, Yokoyama Y, Maemoku H, et al. 2016. Weak monsoon event at 4.2 ka recorded in sediment from Lake Rara, Himalayas. Quaternary International, 397: 349–359, doi: 10.1016/j.quaint.2015.05.053

Nie Baofu, Chen Tegu, Liang Meitao, et al. 1997. Relationship between coral growth rate and sea surface temperature in the northern part of South China Sea during the past 100 a. Science in China Series D: Earth Sciences, 40(2): 173–182, doi: 10.1007/BF02878376

Nie Baofu, Ch en, Te gu, Peng Zicheng. 1999. Reconstruction of sea surface temperature series in the last 220 years by use of reef corals in Xisha waters, South China Sea. Chinese Science Bulletin, 44(22): 2094–2098, doi: 10.1007/BF02884929

Olsen J, Anderson N J, Knudsen M F. 2012. Variability of the North Atlantic oscillation over the past 5, 200 years. Nature Geoscience, 5(11): 808–812, doi: 10.1038/NGEO1589

Ramos-Román M J, Jiménez-Moreno G, Camuera J, et al. 2018. Holocene climate aridification trend and human impact interrupted by millennial- and centennial-scale climate fluctuations from a new sedimentary record from Padul (Sierra Nevada, southern Iberian Peninsula). Climate of the Past, 14(1): 117–137, doi: 10.5194/cp-14-117-2018

Rao Zhiguo, Li Yunxia, Zhang Jiawu, et al. 2016. Investigating the long-term palaeoclimatic controls on the δD and δ¹⁸O of precipitation during the Holocene in the Indian and East Asian monsoonal regions. Earth-Science Reviews, 159: 292–305, doi: 10.1016/j.earscirev.2016.06.007

Roland T P, Caseldine C J, Charman D J, et al. 2014. Was there a "4.2 ka event" in Great Britain and Ireland? Evidence from the peatland record Quaternary Science Reviews, 83: 11–27, doi: 10.1016/j.quascirev.2013.10.024

Ropelewski C F, Halpert M S. 1987. Global and regional scale precipitation patterns associated with the El Niño/Southern Oscillation. Monthly Weather Review, 115(8): 1606–1626, doi: 10.1175/1520-0493(1987)115<1606:GARSPP>2.0.CO;2

Saenger C, Cohen A L, Oppo D W, et al. 2009. Surface-temperature trends and variability in the low-latitude North Atlantic since 1552. Nature Geoscience, 2(7): 492–495, doi: 10.1038/ngeo552

Shi Wei, Ma Chunmei, Zhu Cheng, et al. 2008. Analysis of stratigraphy on multi—profiles in the Taihu Lake region and paleoenvironmental events in the Liangzhu culture epoch. Geographical Research, 27(5): 1129–1138, doi: 10.3321/j.issn:1000-0585.2008.05.016

Staubwasser M, Sirocko F, Grootes P M, et al. 2003. Climate change at

the 4.2 ka BP termination of the Indus valley civilization and Holocene South Asian monsoon variability. Geophysical Research Letters, 30(8): 1425, doi: 10.1029/2002GL016822

Tan Liangcheng, Cai Yanjun, Cheng Hai, et al. 2018a. Centennial- to decadal-scale monsoon precipitation variations in the upper Hanjiang River region, China over the past 6650 years. Earth and Planetary Science Letters, 482: 580–590, doi: 10.1016/j.epsl.2017.11.044

Tan Liangcheng, Shen Chuanchou, Cai Yanjun, et al. 2018b. Great flood in the middle-lower Yellow River reaches at 4000 a BP inferred from accurately-dated stalagmite records. Science Bulletin, 63(4): 206–208, doi: 10.1016/j.scib.2018.01.023

Toth L T, Aronson R B, Cobb K M, et al. 2015. Climatic and biotic thresholds of coral-reef shutdown. Nature Climate Change, 5(4): 369–374, doi: 10.1038/nclimate2541

Toth L T, Aronson R B, Vollmer S V, et al. 2012. ENSO Drove 2500-Year collapse of eastern Pacific Coral reefs. Science, 337(6090): 81–84, doi: 10.1126/science.1221168

Trenberth K E, Caron J M. 2000. The Southern Oscillation revisited: sea level pressures, surface temperatures, and precipitation. Journal of Climate, 13(24): 4358–4365, doi: 10.1175/1520-0442(2000)013<4358:TSORSL>2.0.CO;2

Vásquez-Bedoya L F, Cohen A L, Oppo D W, et al. 2012. Corals record persistent multidecadal SST variability in the Atlantic Warm Pool since 1775 AD. Paleoceanography, 27(3): PA3231, doi: 10.1029/2012PA002313

Walker M J C, Berkelhammer M, Björck S, et al. 2012. Formal subdivision of the Holocene Series/Epoch: a discussion paper by a working group of INTIMATE (Integration of ice-core, marine and terrestrial records) and the Subcommission on Quaternary Stratigraphy (International Commission on Stratigraphy). Journal of Quaternary Science, 27(7): 649–659, doi: 10.1002/jqs.2565

Wang Bin, Wu Renguang, Fu Xiouhua, et al. 2000. Pacific–East Asian teleconnection: how does ENSO affect East Asian climate? Journal of Climate, 13(9): 1517–1536, doi: doi:10.1175/1520-0442(2000)013>1517:PEATHD<2.0.CO;2

Wang Bin, Huang Fei, Wu Zhiwei, et al. 2009. Multi-scale climate variability of the South China Sea monsoon: a review. Dynamics of Atmospheres and Oceans, 47(1–3): 15–37, doi: 10.1016/j.dynatmoce.2008.09.004

Wang Yafei, Li Yan, Li Pingyun, et al. 2008. The large scale circulation of the snow disaster in South China in the beginning of 2008. Acta Meteorologica Sinica, 66(5): 826–835

Wang Hui, Liu Kexiu, Gao Zhigang, et al. 2017. Characteristics and possible causes of the seasonal sea level anomaly along the South China Sea coast. Acta Oceanologica Sinica, 36(1): 9–16, doi: 10.1007/s13131-017-0988-0

Wanner H, Beer J, Bütikofer J, et al. 2008. Mid- to Late Holocene climate change: an overview. Quaternary Science Reviews, 27(19–20): 1791–1828, doi: 10.1016/j.quascirev.2008.06.013

Wanner H, Mercolli L, Grosjean M, et al. 2015. Holocene climate variability and change; a data-based review. Journal of the Geological Society, 172(2): 254–263, doi: 10.1144/jgs2013-101

Wanner H, Solomina O, Grosjean M, et al. 2011. Structure and origin of Holocene cold events. Quaternary Science Reviews, 30(21-22): 3109–3123, doi: 10.1016/j.quascirev.2011.07.010

Weiss H. 2016. Global megadrought, societal collapse and resilience at 4. 2-3.9 ka BP across the Mediterranean and West Asia. Past Global Change Magazine, 24(2): 62–63, doi: 10.22498/pages.24.2.62

Weiss H, Courty M A, Wetterstrom W, et al. 1993. The genesis and collapse of third millennium North Mesopotamian Civilization. Science, 261(5124): 995–1004, doi: 10.1126/science.261.5124.995

Wu Wenxiang, Liu T. 2004. Possible role of the "Holocene Event 3" on the collapse of Neolithic Cultures around the Central Plain of China. Quaternary International, 117(1): 153–166, doi: 10.1016/S1040-6182(03)00125-3

Wu Qinglong, Zhao Zhijun, Liu Li, et al. 2016. Outburst flood at 1920 BCE supports historicity of China's Great Flood and the Xia dynasty. Science, 353(6299): 579–582, doi: 10.1126/science.aaf0842

Wu Xudong, Zhang Zhaohui, Xu Xiaomei, et al. 2012. Asian summer monsoonal variations during the Holocene revealed by Huguangyan maar lake sediment record. Palaeogeography, Palaeoclimatology, Palaeoecology, 323–325: 13–21, doi: 10.1016/j.palaeo.2012.01.020

Xu Hai, Yeager K M, Lan Jianghu, et al. 2015. Abrupt Holocene Indian Summer Monsoon failures: a primary response to solar activity?. The Holocene, 25(4): 677–685, doi: 10.1177/0959683614566252

Yan Mi, Liu Jian. 2019. Physical processes of cooling and megadrought during the 4.2 ka BP event: results from TraCE-21ka simulations. Climate of the Past, 15(1): 265–277, doi: 10.5194/cp-15-265-2019

Yan Hong, Liu Chengcheng, Zhang Wenchao, et al. 2017. ENSO variability around 2000 years ago recorded by Tridacna gigas $\delta^{18}O$ from the South China Sea. Quaternary International, 452: 148–154, doi: 10.1016/j.quaint.2016.05.011

Yan Hong, Sun Liguang, Liu Xiaodong, et al. 2010. Relationship between ENSO events and regional climate anomalies around the Xisha Islands during the last 50 years. Journal of Tropical Oceanography, 29(5): 29–35, doi: 10.3969/j.issn.1009-5470.2010.05.005

Yan Hong, Sun Liguang, Oppo D W, et al. 2011a. South China Sea hydrological changes and Pacific Walker Circulation variations over the last millennium. Nature Communication, 2(1): 293, doi: 10.1038/ncomms1297

Yan Hong, Sun Liguang, Wang Yuhong, et al. 2011b. A record of the Southern Oscillation Index for the past 2,000 years from precipitation proxies. Nature Geoscience, 4(9): 611–614, doi: 10.1038/ngeo1231

Yu Kefu. 2012. Coral reefs in the South China Sea: their response to and records on past environmental changes. Science China Earth Sciences, 55(8): 1217–1229, doi: 10.1007/s11430-012-4449-5

Yu Kefu, Zhao Jianxin, Shi Qi, et al. 2006. U-series dating of dead Porites corals in the South China Sea: Evidence for episodic coral mortality over the past two centuries. Quaternary Geochronology, 1(2): 129–141, doi: 10.1016/j.quageo.2006.06.005

Zhang Huiling. 2013. High-resolution Holocene monsoon climate records in corals and stalagmites (in Chinese) (dissertation). Beijing: University of Chinese Academy of Sciences

Zhang Haiwei, Cheng Hai, Cai Yanjun, et al. 2018. Hydroclimatic variations in southeastern China during the 4.2 ka event reflected by stalagmite records. Climate of the Past, 14(11): 1805–1817, doi: 10.5194/cp-14-1805-2018

Zhang Huiling, Yu Kefu, Shi Qi, et al. 2014. Sea surface temperature variations during the mid-late Holocene reconstructed by Porites coral growth rates in the Xisha Islands. Quaternary Sciences, 34(6): 1296–1305, doi: 10.3969/j.issn.1001-7410.2014.06.19

Zhang Huiling, Yu Kefu, Shi Qi, et al. 2017. Sea surface temperature variations since the industrial revolution as reconstructed by Porites coral growth rate in Xisha Waters. Tropical Geography, 37(5): 701–707

Zhao Yan, Chen Fahu, Zhou Aifeng, et al. 2010. Vegetation history, climate change and human activities over the last 6200 years on the Liupan Mountains in the southwestern Loess Plateau in central China. Palaeogeography, Palaeoclimatology, Palaeoecology, 293(1–2): 197–205, doi: 10.1016/j.palaeo.2010.05.020

Zhou Wen, Chan J C L. 2007. ENSO and the South China Sea summer monsoon onset. International Journal of Climatology, 27(2): 157–167, doi: 10.1002/joc.1380